Supporting Information

Feklistov *et al.* 10.1073/pnas.0802822105

SI Materials and Methods

RNAP Inhibitors. Rifampicin and rifamycin SV were purchased from Sigma. Rifapentine and rifabutin were purchased from Sequoia Research Products. Concentrations of rifamycins were determined spectrophotometrically using ε_{334} = 28,000. Sorangicin was prepared as in ref. 1.

DNA Fragments. Experiments in Fig. 1 and Fig. S4 were performed using a 370-bp DNA fragment comprising positions -193 to +177 of the T7 A1 promoter (obtained by PCR from plasmid pTZ19; ref. 2). Experiments in Fig. 2 and Figs. S5–S7 and in Tables 1 and 2, and Table S1 were performed using an 80-bp DNA fragment comprising positions −50 to +30 of the T5 N25-CONS promoter, a derivative of the T5 N25 promoter having consensus core promoter elements (prepared by mixing equimolar quantities of nontemplate-strand oligodeoxyribonucleotide 5′-TCATAAAAAATTTAT**TTGACA**TCAGGAAAATTTTT**TGG**T**ATAAT**AGATTC*A*TAAATTTGAGAGAGGAGTTTAAATATGGC-3′ and template-strand oligodeoxyribonucleotide 5′-GCCATATTTAAACTCCTCTCTCAAATTTATGAATCT**ATTATA**C**CA**AAAAATTTTCCTGA**TGTCAA**ATAAATTTTTTATGA-3′ in 40 mM Tris·HCl (pH 7.9) and 100 mM NaCl, heating for 2 min at 95°C, and slow cooling to 25°C). The T5 N25-CONS promoter forms stable, productive RP_o with all RNAP derivatives, all rifamycin concentrations, all Mg^{2+} concentrations, and all temperatures analyzed in this work.

Plasmids. Plasmids pIA594 [P_{trc}-(His_6-)*rpoB*^{L1235A}], pIA595 [P_{trc}-(His_6-)*rpoB*], pIA597 [P_{T7}*rpoA*(His_6-)*rpoB*^{L1235A}*C*], and pVS5 [P_{T7}-*rpoABC*(-CBD)*Z*] were obtained from I. Artsimovitch (3, 4). Plasmid pRL706 was obtained from R. Landick (5). Plasmids pRL706^{D516N} [P_{trc}-(His_6-)*rpoB*^{D516N}] and pRL706^{D516V} [P_{trc}-(His_6-)*rpoB*^{D516V}] were constructed from plasmid pRL706 by use of site-directed mutagenesis. Plasmid pEcRNAP1 [P_{T7}-*rpoABCZ*] was constructed from plasmid pVS5 by deletion of the CBD (chitin-binding-domain) coding sequence. Plasmids pEcABC(-H10-HMPK)*Z* [P_{T7}-*rpoABC*(-His_{10}-HMPK)*Z*], pEcA(H10-PPX-)BCZ [P_{T7}-*rpoA*(His_{10}-PPX-)*BCZ*], and pEcA(H10-PPX-)B^{L1235A}CZ [P_{T7}-*rpoA*(His_{10}-PPX-)*B*^{L1235A}*CZ*] were constructed from plasmid pEcRNAP1 by introduction of a His_{10}-HMPK (His_{10} followed by heart-muscle-protein-kinase site, HHHHHHHHHHLRRASV) coding sequence, a His_{10}-PPX (His_{10} followed by linker and PreScission-Protease cleavage site, HHHHHHHHHHSSGLEVLFQGP) coding sequence, and/or an *rpoB* ^{L1235A} allele.

σ^{70}. σ^{70} was prepared as in ref. 6. σ^{70} labeled with fluorescein at position 517 ([F^{517}]σ^{70}) was prepared as in ref. 7.

RNAP Core. Wild-type RNAP core was prepared from strain XE54 transformed with pRL706 (procedures as in ref. 6), was prepared from strain BL21(DE3) (EMD Biosciences) transformed with pEcA(H10-PPX-)BCZ (procedures essentially as above), and was purchased from Epicentre. C-terminally HMPK-tagged wild-type RNAP core was prepared from strain BL21(DE3) (EMD Biosciences) transformed with pEcABC(H6-HMPK)Z (procedures essentially as above). [Asn-516]β-RNAP core and [Val-516]β-RNAP core were prepared from strain XE54 transformed with, respectively, pRL706^{D516N} and pRL706^{D516V} (procedures essentially as above). [Ala-1235]β-RNAP core was prepared from strain XE54 transformed with pIA594 (procedures essentially as above, but using heparin-HiTrap chromatography in place of Mono-Q chromatography), was prepared from strain XL1-Blue (Stratagene) transformed with pIA594 (same procedures), was prepared from strain BL21Star(DE3) (Invitrogen) transformed with pEcA(H10-PPX)B^{L1235A}CZ (same procedures), and was prepared from strain BL21Star(DE3) (Invitrogen) transformed with pEcA(H10-PPX)B^{L1235A}CZ and cultured at 32°C in transformation steps and in subsequent steps (same procedures).

RNAP Holo. Except where noted otherwise, RNAP holo derivatives were prepared as in ref. 6. Except where noted otherwise, complexes of RNAP holo derivatives with rifamycins were prepared by incubation of RNAP holo derivative with rifamycin for ≥3 min at 24°C (≥3 min in experiments with rifamycin concentrations ≥0.5 μM; ≥10 min in experiments with rifamycin concentrations ≥0.04 μM but <0.5 μM; ≥30 min in experiments with rifamycin concentrations ≥0.002 μM but <0.04 μM).

RP_o. Except where noted otherwise, RP_o derivatives for use in transcription experiments were prepared by incubation of 4 nM RNAP holo derivative with 5 nM promoter DNA fragment in buffer A [40 mM Tris·HCl (pH 8.0), 100 mM NaCl, 1 mM DTT, 5% glycerol] containing 10 mM $MgCl_2$ (or other specified concentration of $MgCl_2$) for 20 min at 37°C (20 min at 32°C for experiments in Table S1). Except where noted otherwise, RP_o derivatives for use in binding experiments were prepared by incubation of 2 nM RNAP holo derivative with 5 nM promoter DNA fragment in buffer A containing 10 mM $MgCl_2$ (or other specified concentration of $MgCl_2$) for 20 min at 37°C. Except where noted otherwise, complexes of RP_o derivatives with rifamycins were prepared by preincubation of RNAP holo derivative with rifamycin for ≥3 min at 24°C (≥3 min in experiments with rifamycin concentrations ≥0.5 μM; ≥10 min in experiments with rifamycin concentrations ≥0.04 μM but <0.5 μM; ≥30 min in experiments with rifamycin concentrations ≥0.002 μM but <0.04 μM) before incubation of RNAP holo derivative with promoter DNA fragment.

Fe^{2+}-Mediated Cleavage Experiments. Reaction mixtures (50 μl) for incorporation of ^{32}P at the C-terminal end of the β' subunit within RNAP core contained 0.7 μM C-terminally HMPK-tagged RNAP core, 100 μCi [γ-^{32}P]ATP (3,000 Ci/mmol; PerkinElmer), and 30 units of calf heart muscle protein kinase (Sigma) in 10 mM Hepes (pH 8.0), 100 mM NaCl, 6 mM $MgCl_2$, and 1 mM DTT. Reactions were allowed to proceed for 20 min at 37°C, reaction mixtures were supplemented with 40 μg of BSA, and the resulting ^{32}P-labeled RNAP core was desalted on a G-50 QuickSpin column (Roche) preequilibrated with 10 mM Hepes (pH 8.0) and 200 mM NaCl (yield = ≈30 pmol; ≈0.3 μCi/pmol). To prepare ^{32}P-labeled RNAP holo, a 2-fold molar excess of σ^{70} was added, and the reaction mixture was incubated 10 min on ice. To prepare ^{32}P-labeled RP_o, a 2-fold molar excess of promoter DNA fragment was added, and the reaction mixture was incubated 10 min at 37°C.

Reaction mixtures for Fe^{2+}-mediated cleavage (20 μl) contained 25 nM ^{32}P-labeled RNAP holo or ^{32}P-labeled RP_o in 10 mM Hepes (pH 8.0), 200 mM NaCl, and the specified concentration of $MgCl_2$ (0–10 mM). Reaction mixtures were supplemented by addition of rifamycin to the specified final concentration and were incubated 15 min at 37°C. Fe^{2+}-mediated cleavage was initiated by the addition of freshly prepared

$(NH_4)_2Fe(SO_4)_2$ (Sigma) to a final concentration of 0–50 μM and DTT to a final concentration of 5 mM, reactions were allowed to proceed 20 min at 25°C (for ^{32}P-labeled RNAP holo) or 10 min at 37°C (for ^{32}P-labeled RP_o), and reactions were terminated by addition of 5 μl of 5% SDS/5 mM EDTA/1% 2-mercaptoethanol/50% glycerol and heating for 10 min at 65°C. Reaction products were separated on 7% Tris-Glycine SDS/PAGE slab gels (20 cm × 20 cm) and were quantified by storage-phosphor imaging (Storm 860; Molecular Dynamics). The fraction of cleavage, F, was defined as the quantity of radioactivity in the band corresponding to the main cleavage product (arising from cleavage within the β' NADFDGD motif; cleavage product VI of ref. 8; bracketed band 1 of Fig. S4) divided by the total amount of radioactivity in the lane (bracketed bands 2 of Fig. S4). Equilibrium dissociation constants for Fe^{2+}–RNAP interaction, K_d^{Fe}, were calculated by fitting data to

$$F = F_{max}[Fe^{2+}]/(K_d^{Fe} + [Fe^{2+}]),$$

where F is the fraction of cleavage at the specified concentration of Fe^{2+}, $[Fe^{2+}]$, F_{max} is the fraction of cleavage at a saturating concentration of Fe^{2+}, and K_d^{Fe} is the equilibrium dissociation constant for Fe^{2+}–RNAP interaction. Equilibrium dissociation constants for Mg^{2+}–RNAP interaction, K_d^{Mg}, were calculated by fitting data to

$$F = F_o(IC_{50})/(IC_{50} + [Mg^{2+}])$$

and

$$K_d^{Mg} = IC_{50}/(1 + [Fe^{2+}]/K_d^{Fe}),$$

where F is the fraction of cleavage at the specified concentration of Mg^{2+}, $[Mg^{2+}]$, F_o is the fraction of cleavage in the absence of Mg^{2+}, and IC_{50} is the concentration of Mg^{2+} at which $F = F_o/2$.

Transcription-Inhibition Assays. Transcription experiments in Fig. 1 and Fig. S4 were performed as follows. Reaction mixtures (10 μl) contained ≈10 nM RP_o in the presence of 0–1.2 μM rifampicin in 40 mM Tris·HCl (pH 7.9)/40 mM KCl/10 mM $MgCl_2$ at 37°C. Reactions were initiated by addition of 4 μl of a solution containing 5 μCi [α-^{32}P]UTP (3,000 Ci/mmol; PerkinElmer), 5 μM UTP, 50 μM ATP, 50 μM CTP, and 50 μM GTP; were allowed to proceed for 10 min at 37°C; and were terminated by addition of 10 μl of 10 M urea/10 mM EDTA. Products were heated for 3 min at 96°C, resolved by urea-PAGE (9), and quantified using a storage-phosphorimaging scanner (Storm 860; Molecular Dynamics). Transcription experiments in Fig. 2, Figs. S5 and S7, Table 2, and Table S1 were performed as follows. Reaction mixtures (18 μl) contained ≈2 nM RP_o in the presence of 0–0.6 μM rifampicin in buffer A containing 10 mM $MgCl_2$ (or other specified $MgCl_2$ concentration) at 37°C (32°C for experiments in Table S1). Reactions were initiated by addition of 2 μl of 10 μCi [α-^{32}P]UTP (6,000 Ci/mmol, PerkinElmer), 0.5 mM UTP, 0.5 mM ATP, 0.5 mM CTP, and 0.5 mM GTP; were allowed to proceed for 20 min at 37°C (32°C for experiments in Table S1); and were terminated by addition of 10 μl of 80% formamide, 10 mM EDTA, 0.04% bromophenol blue, and 0.04% xylene cyanol. Products were heated 5 min at 90°C, resolved by urea-PAGE (9), and quantified using storage-phosphor imaging (Storm 860; Molecular Dynamics). IC_{50} values were extracted by fitting data to

$$IC_{50} = \frac{[Rif - RP_o(1 - Y/Y_o)](Y/Y_o)}{1 - Y/Y_o},$$

where Rif is the concentration of rifamycin, RP_o is the concentration of RNAP–promoter open complex, Y is the yield of the run-off transcript at the specified concentration of rifamycin, and Y_o is the yield of run-off transcript in the absence of rifamycin.

Transcription experiments in Fig. S6 and Table 1 were performed by the procedure in the preceding paragraph, but using a reaction time of 2 min and a reaction temperature of 24°C for RNA synthesis, and using ≈20 nM RP_o. {The use of a comparatively short reaction time for RNA synthesis was necessary in these experiments to avoid underestimation of the efficiency of inhibition of transcription by rifampicin due to dissociation of rifampicin from [Asn-516]β-RNAP (k_{off} = 0.013 s^{-1}; Table 2) and [Val-516]β-RNAP (k_{off} = 0.17 s^{-1}; Table 2) during the course of RNA synthesis. The use of a comparatively high concentration of RP_o was necessary in these experiments to obtain measurable RNA yields with the comparatively short reaction time for RNA synthesis.}

Growth-Inhibition Assays: Liquid Medium. Single colonies of strain DH5α (Invitrogen) or strain D21f2/tolC (10) transformed with pIA595 or pIA594 were inoculated into 5 ml of LB (9) containing 100 μg/ml ampicillin, were cultured for 3.5 h at 7°C with shaking (32°C for experiments in Table S1), were supplemented with IPTG to 1 mM, and were cultured for an additional 1 h at 37°C with shaking (32°C for experiments in Table S1). Diluted aliquots (each containing 10^6 cells in 100 μl of LB containing 100 μg/ml ampicillin, 1 mM IPTG, and the specified concentration of rifamycin) were added to wells of a 96-well microplate and were cultured for 16 h at 37°C with shaking (32°C for experiments in Table S1). Concentrations of rifamycins were 0, 0.0125, 0.025, 0.05, 0.1, 0.2, 0.4, 0.8, 1.6, and 3.2 μg/ml for experiments with transformants of strain DH5α and were 0, 3.125, 6.25, 12.5, 25, 50, 100, 200, and 400 μg/ml for experiments with transformants of strain D21f2/tolC. The minimal inhibitory concentration (MIC) was defined as the lowest concentration of rifamycin that reduced culture density (assessed by measurement of OD_{600}) by ≥90%.

Growth-Inhibition Assays: Solid Medium. Single colonies of strain DH5α (Invitrogen) or strain D21f2/tolC (10) transformed with pIA595 or pIA594 were inoculated into 5 ml of LB containing 100 μg/ml ampicillin, were cultured for 3.5 h at 37°C with shaking (32°C for experiments in Table S1), were supplemented with IPTG to 1 mM, and were cultured for an additional 1 h at 37°C with shaking (32°C for experiments in Table S1). Diluted aliquots (each containing 10^7 cells in 100 μl LB containing 1 mM IPTG) were applied to LB-agar plates (9) containing 100 μg/ml ampicillin and 1 mM IPTG, a rifampicin (high-range) Etest strips (AB BIODISK) was placed on each plate, and each plate was incubated for 16 h at 37°C (32°C for experiments in Table S1). The minimal inhibitory concentration (MIC)e was determined from the intersection of the zone of growth inhibition with the concentration scale on the Etest strip.

Rifamycin–RNAP Interaction Assays: Fluorescence-Quenching Measurements. It previously has been shown that rifamycin–RNAP interaction can be detected by monitoring quenching of fluorescence emission of a fluorescent probe incorporated site-specifically into RNAP (serving as fluorescence resonance energy transfer donor) by the naphthyl group of rifamycin [serving as fluorescence resonance energy transfer acceptor (7)]. In this work, this approach was used to determine association kinetics, dissociation kinetics, and equilibrium dissociation constants for rifamycin–RNAP interaction. Experiments were performed using RNAP holo and RP_o derivatives having the fluorescent probe fluorescein incorporated site-specifically at residue of 517 of σ^{70} ([F^{517}]σ^{70}-RNAP holo and [F^{517}]σ^{70}-RP_o derivatives; methods as in ref. 7). Interaction of rifamycins with [F^{517}]σ^{70}-RNAP holo and [F^{517}]σ^{70}-RP_o derivatives results in highly efficient, readily measurable, quenching of fluorescence emis-

sion (efficiencies of quenching at saturation = 60–75%) (7) (V.M. and R.H.E., unpublished results). Steady-state and kinetic fluorescence measurements were performed using a QuantaMaster QM1 spectrofluorometer (PTI) (excitation wavelength = 480 nm; emission wavelength = 530 nm; and excitation and emission slit widths = 5 nm).

Parallel experiments were performed using RNAP holo derivatives having the fluorescent probe fluorescein incorporated site-specifically at residue 36, at residue 59, at residue 459, or at residue 517 of σ^{70} (methods as in ref. 7); there was no detectable effect of the labeling-site position on association kinetics, dissociation kinetics, or equilibrium dissociation constants.

Rifamycin–RNAP Interaction Assays: Association Kinetics. For determination of association kinetics, 720 μl of 2 nM [F^{517}]σ^{70}-RNAP holo derivative or [F^{517}]σ^{70}-RPo derivative in buffer A containing 10 mM $MgCl_2$ (or other specified concentration of $MgCl_2$) and 0.02% Tween-20 at 24°C was mixed with 30 μl of 0.01–3.5 μM rifamycin in the same buffer at 24°C, in a cuvette chamber with a mixing dead time of ≈0.5 s, and fluorescence emission intensities were monitored for 3–30 min at 24°C. With wild-type RNAP holo and 10 mM $MgCl_2$, the times required for complete association were ≈20, ≈10, ≈4, and ≈1 min at, respectively, 0.01, 0.02, 0.05, and 0.5 μM rifampicin. With wild-type RP_o and 10 mM $MgCl_2$, the times required for complete association were >60 min at 0.01–0.5 μM rifampicin. On-rates for rifamycin–RNAP interaction, k_{on}, were calculated by fitting data to

$$I = (I_o - I_\infty)\exp(-k_{obs}t) + I_\infty,$$

where k_{obs} is the observed association rate constant at a specified concentration of rifamycin, I is the fluorescence emission intensity at time t, I_o is the fluorescence emission intensity at $t = 0$, and I_∞ is the fluorescence emission intensity at $t = \infty$; followed by fitting the dependence of k_{obs} on the concentration of rifamycin, [Rif], to

$$k_{obs} = k_{on}[\mathrm{Rif}] + k_{off},$$

where k_{off} is ≥0 but is otherwise unconstrained.

Rifamycin–RNAP Interaction Assays: Dissociation Kinetics. The RNAP inhibitor sorangicin A binds to the same site on RNAP as rifamycins (1) and competes with rifamycins for binding to RNAP (1, 11) (V.M., H.I., R.J., and R.H.E., unpublished data). The affinity of sorangicin A for RNAP is comparable to the affinity of rifamycins for RNAP ($K_d^{\text{sorangicin}}/K_d^{\text{rifampicin}} \sim 1$) (11) (V.M., H.I., R.J., and R.H.E., unpublished data). Sorangicin A, unlike rifamycins, has negligible absorbance at wavelengths >400 nm; therefore, binding of sorangicin A to [F^{517}]σ^{70}-RNAP holo and [F^{517}]σ^{70}-RP_o derivatives, unlike binding of rifamycins to [F^{517}]σ^{70}-RNAP holo and [F^{517}]σ^{70}-RP_o derivatives, results in negligible quenching of fluorescence emission (quenching efficiency <5%) (V.M., H.I., R.J., and R.H.E., unpublished data). In this work, we have exploited these properties of sorangicin A to use sorangicin A as a "competitor trap" for measurements of rifamycin dissociation kinetics.

For determination of dissociation kinetics, 720 μl of 2 nM [F^{517}]σ^{70}-RNAP holo derivative or [F^{517}]σ^{70}-RPo derivative preequilibrated with 0.05 or 0.2 μM rifamycin in buffer A containing 10 mM $MgCl_2$ (or other specified concentration of $MgCl_2$) and 0.02% Tween 20 at 24°C was mixed with 30 μl of 12.5 or 50 μM sorangicin in the same buffer at 24°C, in a cuvette chamber with a mixing dead time of ≈0.5 s, and fluorescence emission intensities were monitored for 5–300 min at 24°C. The final concentrations of rifamycin and sorangicin A were 0.05 and 0.5 μM for most experiments but were 0.2 and 2 μM for experiments with [Val-516]β-[F^{517}]σ^{70}-RNAP holo (for which higher concentrations of rifamycin were required to achieve significant binding of rifamycin). Dissociation kinetics were found not to depend on the concentration of sorangicin A in the concentration range used in this work (final concentrations of 0.5–2 μM), indicating that sorangicin A in this concentration range does not actively displace rifamycins from RNAP but, instead, binds free RNAP only after rifamycins dissociate from RNAP. Off-rates for rifamycin–RNAP interaction, k_{off}, were calculated as

$$I = I_o + (I_\infty - I_o)[1 - \exp(-k_{off}t)],$$

where I is the fluorescence emission intensity at time t, I_o is the fluorescence intensity at $t = 0$, and I_∞ is the fluorescence intensity at $t = \infty$.

Rifamycin–RNAP Interaction Assays: Equilibrium Dissociation Constants. Equilibrium dissociation constants for rifamycin–RNAP interaction, K_d, were calculated as k_{off}/k_{on}. For [Asn-516]β-RNAP and [Val-516]β-RNAP, values of K_d independently were determined using equilibrium binding assays. (For [Asn-516]β-RNAP and [Val-516]β-RNAP, unlike for wild-type RNAP, values of K_d are sufficiently high to permit accurate determination of K_d in equilibrium binding assays.) For equilibrium binding assays, 735 μl of 1 nM [F^{517}]σ^{70}-RNAP holo derivative in buffer A containing 10 mM $MgCl_2$ and 0.02% Tween 20 at 24°C was mixed with 15 μl of 0–25 μM rifampicin in the same buffer at 24°C, and fluorescence emission intensities were measured after 10 min at 24°C. Efficiencies of fluorescence resonance energy transfer (E) and fractional saturations (θ) were calculated as

$$E = 1 - I/I_x$$

$$\theta = E/E_{max},$$

where I and I_x are fluorescence emission intensities before and after addition of rifampicin (corrected for inner filter effects and for nonspecific RNAP–rifampicin interactions by subtraction of corresponding values in experiments in the presence of a 10-fold excess of sorangicin), and E_{max} is E at saturation (determined in experiments using wild-type [F^{517}]σ^{70}-RNAP holo). Equilibrium dissociation constants, K_d, were extracted by fitting data to

$$\theta = [\mathrm{Rif}]/(K_d + [\mathrm{Rif}]),$$

where [Rif] is the concentration of rifampicin. Values of K_d obtained from equilibrium binding assays were comparable to values of K_d obtained from association and dissociation kinetics (Table 1, center columns).

1. Campbell EA, *et al.* (2005) Structural, functional, and genetic analysis of sorangicin inhibition of bacterial RNA polymerase. *EMBO J* 24:674–682.
2. Nudler E, Goldfarb A, Kashlev M (1994) Discontinuous mechanism of transcription elongation. *Science* 265:793–796.
3. Artsimovitch I, Svetlov V, Murakami KS, Landick R (2003) Co-overexpression of *Escherichia coli* RNA polymerase subunits allows isolation and analysis of mutant enzymes lacking lineage-specific sequence insertions. *J Biol Chem* 278:12344–12355.
4. Artsimovitch I, *et al.* (2005) Allosteric modulation of the RNA polymerase catalytic reaction is an essential component of transcription control by rifamycins. *Cell* 122:351–363.
5. Severinov K, Mooney R, Darst SA, Landick R (1997) Tethering of the large subunits of *Escherichia coli* RNA polymerase. *J Biol Chem* 272:24137–24140.
6. Mukhopadhyay J, *et al.* (2003) Fluorescence resonance energy transfer (FRET) in analysis of transcription-complex structure and function. *Methods Enzymol* 371:144–159.
7. Knight J, Mekler V, Mukhopadhyay J, Ebright RH, Levy R (2005) Distance-restrained docking of rifampicin and rifamycin SV to RNA polymerase using systematic FRET measurements: Developing benchmarks of model quality and reliability. *Biophys J* 88:925–938.
8. Mustaev A, *et al.* (1997) Modular organization of the catalytic center of RNA polymerase. *Proc Natl Acad Sci USA* 94:6641–6645.

9. Sambrook J, Fritsch E, Maniatis T (1989) *Molecular Cloning: A Laboratory Manual* (Cold Spring Harbor Lab Press, Cold Spring Harbor, NY).
10. Fralick J, Burns-Keliher L (1994) Additive effect of tolC and rfa mutations on the hydrophobic barrier of the outer membrane of *Escherichia coli* K-12. *J Bacteriol* 176:6404–6406.
11. Xu M, Zhou Y, Goldstein B, Jin DJ (2005) Cross-resistance of *Escherichia coli* RNA polymerases conferring rifampin resistance to different antibiotics. *J Bacteriol* 187:2783–2792.

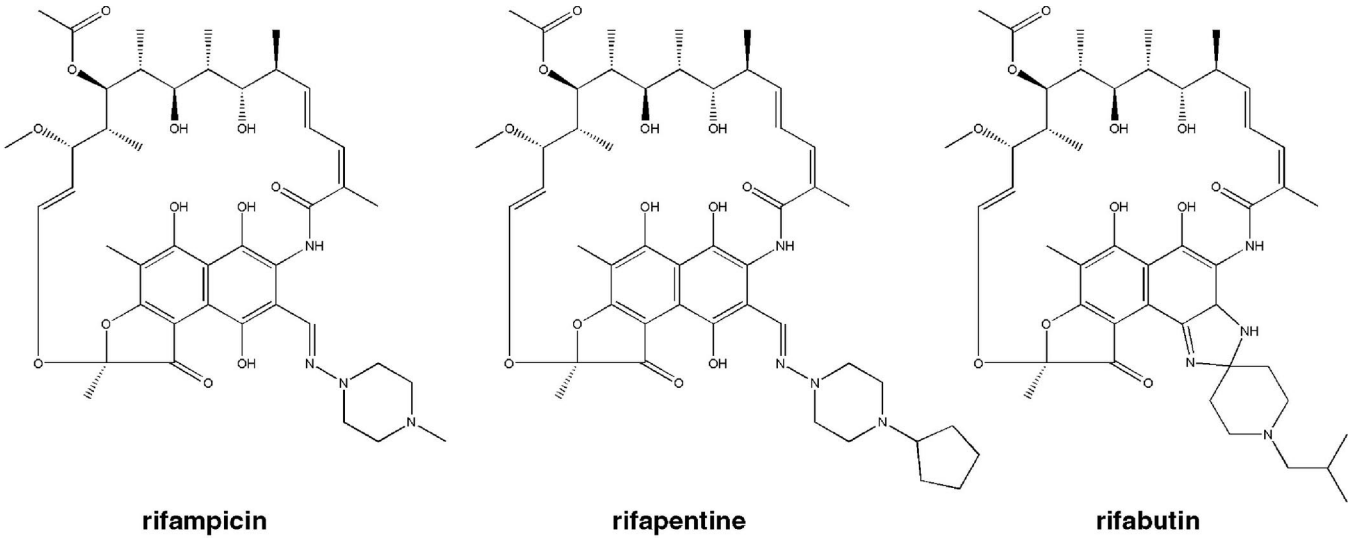

Fig. S1. Rifamycins. Structures are shown for rifampicin (also known as rifampin; *Left*), rifapentine (*Center*), and rifabutin (*Right*). Unless specified otherwise, data presented in this report are from experiments performed with rifampicin. Experiments performed with rifapentine and rifabutin yield equivalent results.

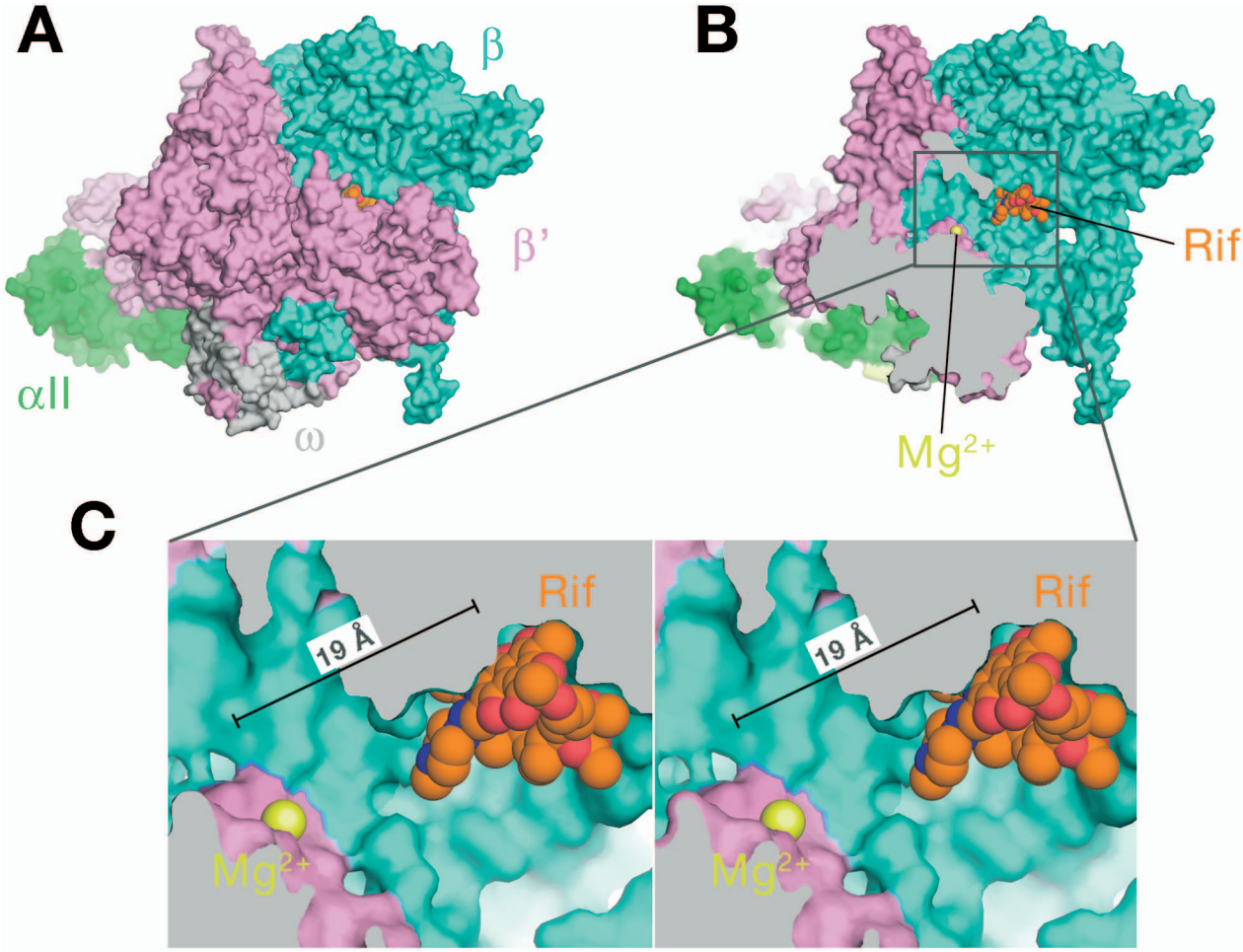

Fig. S2. Rifamycin–RNAP interaction. Structure of rifampicin in complex with *Thermus aquaticus* RNAP (1) [Protein Data Bank (PDB) entry 1I6V]. RNAP is shown as a molecular surface, with the α^{I} subunit in yellow, α^{II} subunit in green, β subunit in cyan, β' subunit in pink, and ω subunit in gray. Rifampicin, where visible, is shown in a van der Waals representation, with carbon atoms in orange, oxygen atoms in red, and nitrogen atoms in blue. The RNAP active-center Mg^{2+}, where visible, is shown as a yellow sphere. (*A*) Full structure. (*B*) Structure with a segment of RNAP (the ''clamp'') cut away to show the interior of the RNAP active-center cleft, containing rifampicin and the RNAP active-center Mg^{2+}. (*C*) Stereoview of a portion of the structure containing rifampicin and the RNAP active-center Mg^{2+}. The distance between the rifampicin center of mass and the RNAP active-center Mg^{2+} is 19 Å.

1. Campbell EA, *et al.* (2001) Structural mechanism for rifampicin inhibition of bacterial RNA polymerase. *Cell* 104:901–912.

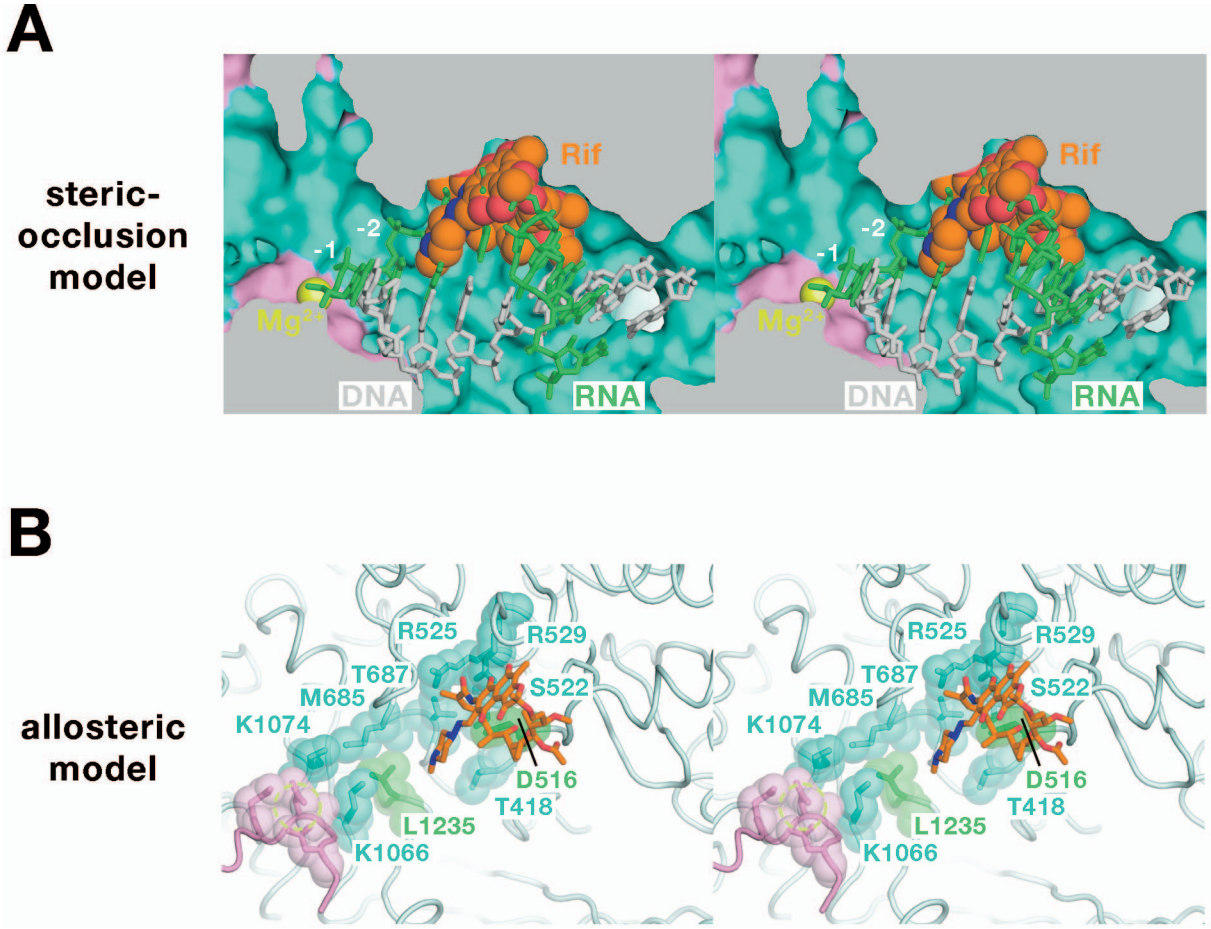

Fig. S3. Mechanistic models for inhibition of RNAP by rifamycins. Stereoviews of the RNAP active-center cleft (view orientations essentially as in Fig. S2C). Except where noted otherwise, colors are as in Fig. S2. (*A*) Steric-occlusion model. Structure of rifampicin in complex with RNAP (1) (PDB entry 1I6V) and, superimposed thereon, the structure of the DNA template strand and RNA product in a transcription complex (2) (PDB entry 2O5I), showing the proposed steric clash between rifampicin and nucleotides −3 to −5 of the RNA product. DNA is in gray; RNA is in green; RNA nucleotides are numbered −1 and −2 starting from the 3′ terminus. (*B*) Allosteric model. Structure of rifampicin in complex with RNAP (1) (PDB entry 1I6V) with the RNAP active-center Mg^{2+} omitted (yellow dashed open circle), showing the proposed pathway of allosteric communication between rifampicin and the and the RNAP active center. Residues of the proposed pathway of allosteric communication are in van der Waals representations and are numbered as in *E. coli* RNAP β subunit. Residues β516 and β1235 are in green.

1. Campbell EA, *et al.* (2001) Structural mechanism for rifampicin inhibition of bacterial RNA polymerase. *Cell* 104:901–912.
2. Vassylyev D, Vassylyeva M, Perederina A, Tahirov T, Artsimovitch I (2007) Structural basis for transcription elongation by bacterial RNA polymerase. *Nature* 448:157–162.

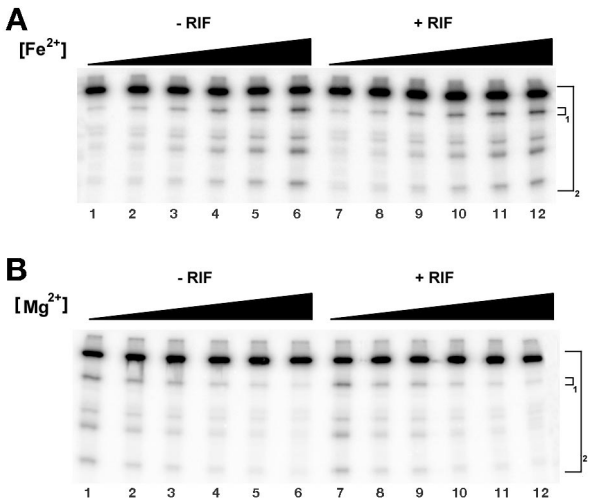

Fig. S4. Absence of effects of rifamycins on metal-ion binding. (*A*) Absence of effects of rifamycins on Fe^{2+} binding (as inferred from measurement of Fe^{2+}-mediated cleavage within the RNAP β' subunit NADFDGD motif as a function of Fe^{2+} concentration). Data are presented for experiments with RP_o in the absence of rifampicin (lanes 1–6) and in the presence of 1.2 μM rifampicin. Fe^{2+} concentrations were 0, 1, 2, 5, 10, and 20 μM in lanes 1–6 and in lanes 7–12. The fraction of cleavage (Fig. 1) was defined as the quantity of radioactivity in the band corresponding to the main cleavage product (arising from cleavage within the β' NADFDGD motif; cleavage product VI of ref. 8; bracketed band 1) divided by the total amount of radioactivity in the lane (bracketed bands 2). (*B*) Absence of effects of rifamycins on Mg^{2+} binding (as inferred from measurement of Fe^{2+}-mediated cleavage within the RNAP β' subunit NADFDGD motif as a function of competing Mg^{2+} concentration). Data are presented for experiments with RP_o in the absence of rifampicin (lanes 1–6) and in the presence of 1.2 μM rifampicin. The Fe^{2+} concentration was 5 μM in all lanes. Mg^{2+} concentrations were 0, 1, 2, 5, 10, and 20 μM in lanes 1–6 and in lanes 7–12. The fraction of cleavage (Fig. 1) was defined as the quantity of radioactivity in the band corresponding to the main cleavage product (arising from cleavage within the β' NADFDGD motif; cleavage product VI of ref. 8; bracketed band 1) divided by the total amount of radioactivity in the lane (bracketed bands 2).

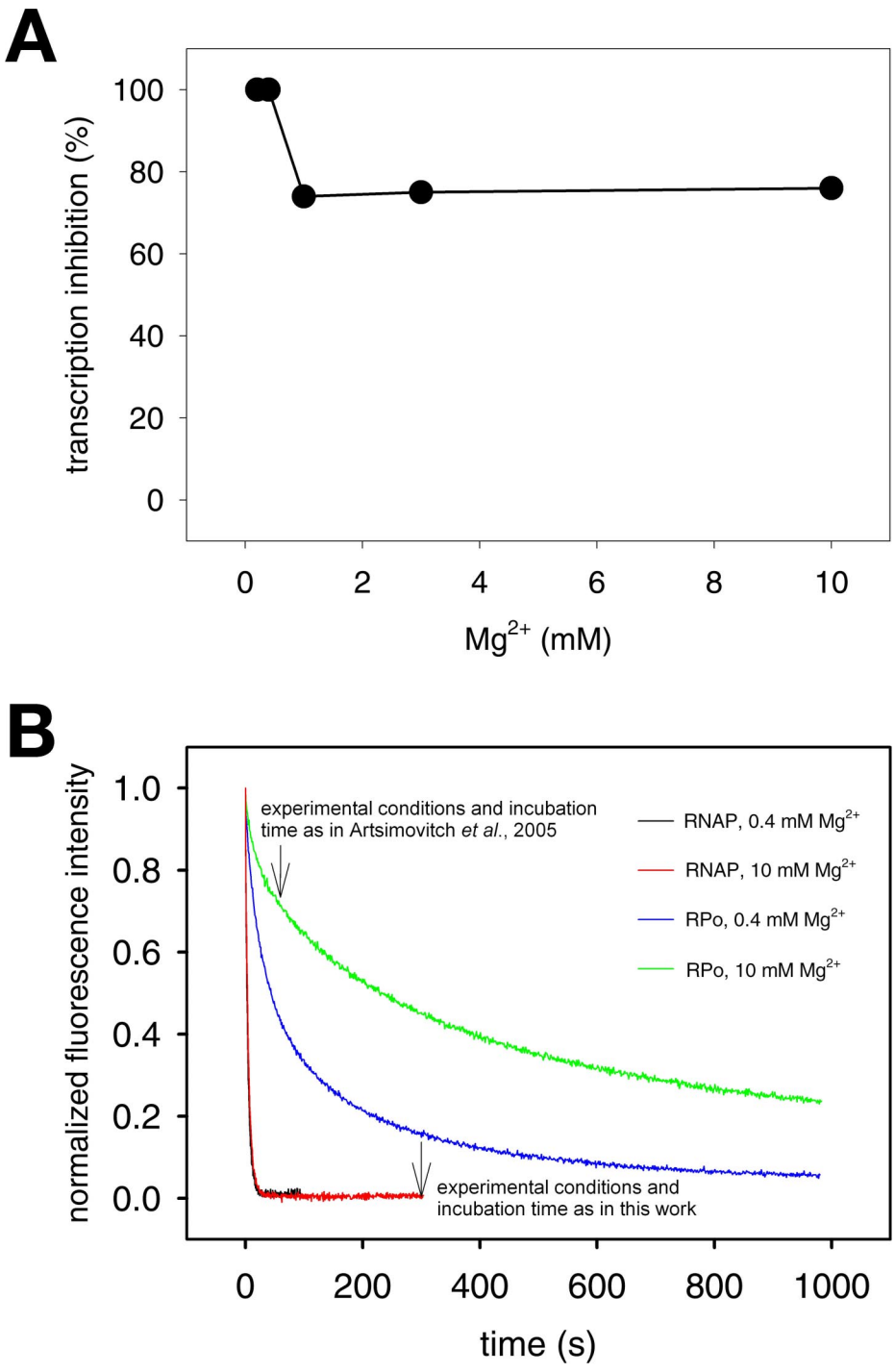

Fig. S5. Reevaluation of experimental design used by Artsimovitch *et al.* (1) to assess effects of Mg^{2+} on rifamycin function. (*A*) Effects of Mg^{2+} on transcription inhibition by rifampicin as assessed using the experimental design of Artsimovitch *et al*. Data are from experiments with preincubation of 0.5 μM rifampicin with RP_o for 1 min. Data are reported as $(Y_o/Y)100\%$, where Y is the yield of run-off transcript at the specified Mg^{2+} concentration, and Y_o is the yield of run-off transcript at the lowest tested Mg^{2+} concentration (0.4 mM). (*B*) Association kinetics for rifampicin–RNAP interaction and relationship to the experimental design of Artsimovitch *et al.* (4). Data are presented for RP_o at 0.4 and 10 mM Mg^{2+} (blue and green lines) and for RNAP holo at 0.4 and 10 mM Mg^{2+} (black and red lines). The arrow at top indicates the experimental conditions and incubation time used for rifamycin–RNAP interaction in Artsimovitch *et al.* (incubation of 0.5 μM rifampicin with RP_o for 1 min; an experimental design that does not yield complete association at 0.4 and 10 mM Mg^{2+} and that yields different extents of association at 0.4 and 10 mM Mg^{2+}: ≈50% and ≈25%). The arrow at bottom indicates the experimental conditions and incubation time used for rifamycin–RNAP interaction in this work (incubation of 0.5 μM rifampicin with RNAP holo for 5 min; an experimental design that yields complete association at 0.4 and 10 mM Mg^{2+}).

1. Artsimovitch I, *et al.* (2005) Allosteric modulation of the RNA polymerase catalytic reaction is an essential component of transcription control by rifamycins. *Cell* 122:351–363.

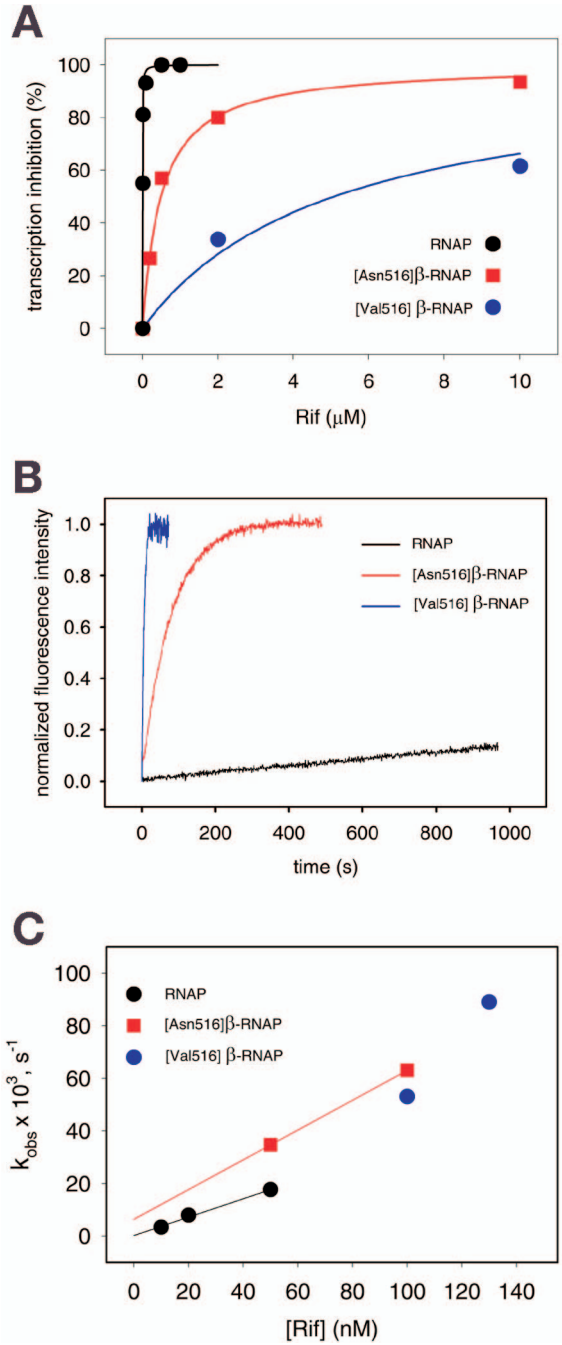

Fig. S6. Absence of putative allosteric effects of classic mutants β-D516N and β-D516V. (*A*) Transcription inhibition by rifampicin: RNAP, [Asn-516]β-RNAP, and [Val-516]β-RNAP. (*B*) Dissociation kinetics for rifampicin–RNAP interaction: RNAP, [Asn-516]β-RNAP, and [Val-516]β-RNAP. (*C*) Association kinetics for rifampicin–RNAP interaction: RNAP, [Asn-516]β-RNAP, and [Val-516]β-RNAP.

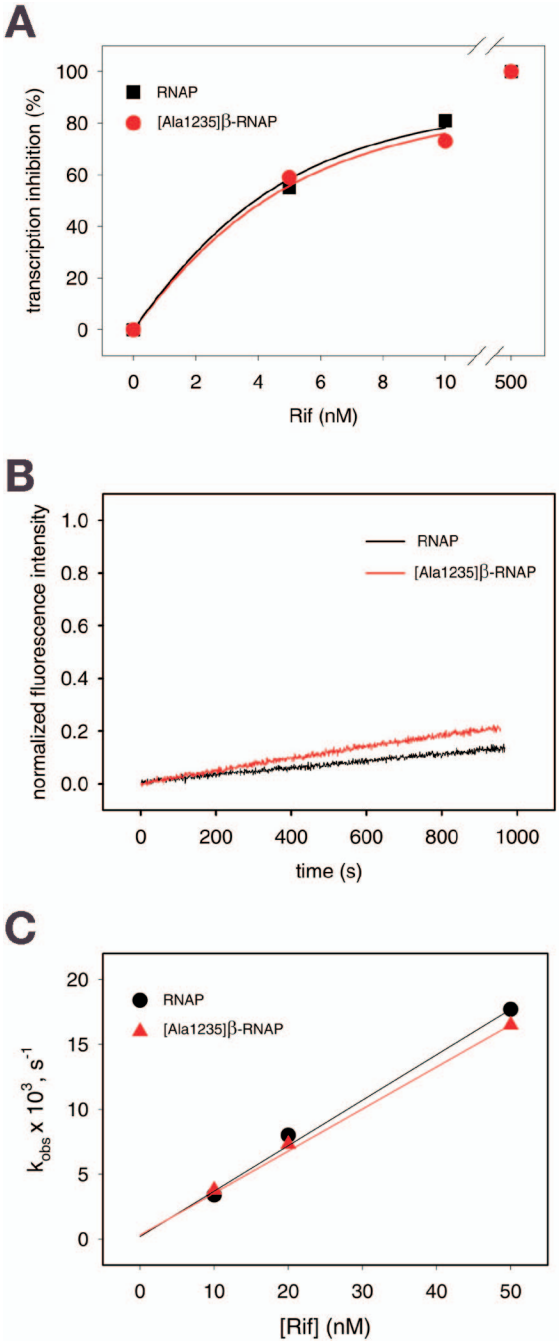

Fig. S7. Absence of putative allosteric effects of designed mutant β-L1235A. (*A*) Transcription inhibition by rifampicin: RNAP and [Ala-1235]β-RNAP. (*B*) Dissociation kinetics for rifampicin–RNAP interaction: RNAP and [Ala-1235]β-RNAP. (*C*) Association kinetics for rifampicin–RNAP interaction: RNAP and [Ala-1235]β-RNAP.

Table S1. Absence of allosteric effects of designed mutant β-L1235A: Parallel experiments at 32°C

RNAP derivative	Liquid medium		Solid medium					
	MIC,* μg/ml	MIC ratio	MIC, μg/ml	MIC ratio	I_{SAT},† %	$I_{SAT,X}/I_{SAT,RNAP}$	IC_{50},‡ nM	$IC_{50_X}/IC_{50_{RNAP}}$
Growth inhibition by rifampicin (*E. coli* strain DH5α)								
RNAP	3.125	[1]	8	[1]				
[Ala1235]β-RNAP	6.25	2	8	1				
Growth inhibition by rifampicin (*E. coli* strain D21f2/tolC)								
RNAP	0.195	[1]	1	[1]				
[Ala1235]β-RNAP	0.098	0.5	0.5	0.5				
Transcription inhibition by rifampicin								
RNAP					100	[1]	3	[1]
[Ala1235]β-RNAP					100	1	4	1

Bacterial growth was assayed at 32°C; transcription was assayed at 32°C using RNAP derivatives purified from cells grown at 32°C.
*MIC is the concentration of rifampicin resulting in 90% inhibition of growth.
†I_{SAT} is the percent inhibition of transcription at a saturating concentration of rifampicin.
‡IC_{50} is the concentration of rifampicin (unbound rifampicin only) resulting in 50% inhibition of transcription.

Table S2. Absence of allosteric effects of designed mutant β-L1235A: Growth inhibition by rifapentine, rifabutin, and rifamycin SV

	Rifapentine		Rifabutin		Rifamycin SV	
RNAP derivative	MIC,* μg/ml	MIC ratio	MIC, μg/ml	MIC ratio	MIC, μg/ml	MIC ratio
Growth inhibition by rifapentine, rifabutin, and rifamycin SV (*E. coli* strain DH5α)						
RNAP	12.5	[1]	12.5	[1]	400	[1]
[Ala1235]β-RNAP	25	2	25	2	400	1
Growth inhibition by rifapentine, rifabutin, and rifamycin SV (*E. coli* strain D21f2/tolC)						
RNAP	0.098	[1]	0.049	[1]	0.781	[1]
[Ala1235]β-RNAP	0.195	2	0.049	1	0.781	1

*MIC is the concentration of rifamycin derivative resulting in 90% inhibition of growth.